Feasibility studies for measuring electrical conductivity of the quark-gluon plasma in heavy-ion collisions with ALICE 3

Bachelor thesis

Clara Melisande Peter

July, 2023

Institut für Kernphysik

Erstgutachter
Prof. Dr. Harald Appelshäuser

Zweitgutachterin
Dr. Raphaelle Bailhache

Contents

1 Introduction **1**

2 Physical Foundations **2**

2.1 Standard model . . . 2
2.2 Quantum chromodynamics . . . 3
2.3 Evolution of the QGP . . . 4
2.4 Dileptons . . . 5
2.4.1 Spectral function . . . 6
2.4.2 Electrical conductivity . . . 7
2.4.3 Direct dielectrons . . . 9
2.4.4 Hadronic background . . . 9
2.4.5 Electromagnetic background . . . 9

3 ALICE 3 **11**

3.1 Magnetic field . . . 12
3.2 TOF system . . . 13
3.3 RICH detector . . . 14

4 Analysis **16**

4.1 Expected thermal signal . . . 16
4.2 Expected hadronic background . . . 17
4.3 Expected electromagnetic background . . . 18
4.3.1 STARlight . . . 18
4.3.2 $p_{\mathrm{T,ee}}$- and m_{ee}-spectrum . . . 20
4.4 Normalisation . . . 22
4.5 Comparison of contributions . . . 23

5 Conclusion **28**

6 Appendix **30**

6.1 Rapidity distribution of ultra-peripheral collisions and hadronic overlaps . . . 30

Bibliography **31**

1 Introduction

In relativistic heavy-ion collisions a state of hot deconfined matter, the quark-gluon plasma (QGP) is produced. This state can only be created and observed at large particle accelerators such as the Large Hadron Collider (LHC) at CERN (**C**onseil **e**uropéen pour la **r**echerche **n**ucléaire) in France and Switzerland, the most powerful accelerator of the world. An experiment at the LHC to further investigate properties of the QGP is ALICE (**A** **L**arge **I**on **C**ollider **E**xperiment).

Planned for the mid-2030s is a new setup for the ALICE experiment. ALICE 3 will continue to observe and investigate fundamental properties of the QGP such as its electrical conductivity. This property is so far unknown for the hadronic and partonic matter and there are no experimental constraints. A possible signal could be measured in the dielectron channel. Dielectrons, correlated positron-electron pairs, are important messengers of the QGP. Since they do not interact strongly with the medium and are produced in all stages of the collision they carry information about the evolution of the medium.

This work will investigate possible background sources that have to be understood in order to extract experimentally the signal expected from the electrical conductivity.

2 Physical Foundations

2.1 Standard model

The standard model (Fig. 2.1) contains all known elementary particles and describes three of the four fundamental interactions, the electromagnetic and weak force, united and described by the electroweak force, and the strong force.

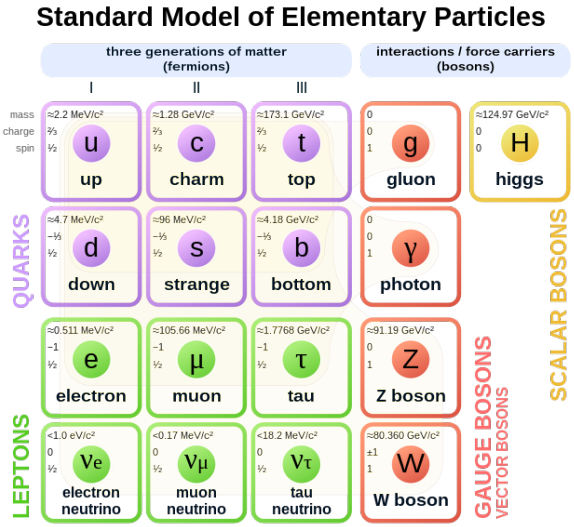

Figure 2.1: Standard model of particle physics [1].

The fundamental particles of the standard model are divided into fermions (and anti-fermions with opposite charges), which have a half-integer spin ($\frac{1}{2}$), and bosons, which have an integer spin (1, 0).

Fermions can be further classified into quarks and leptons. Both are subdivided into three generations (each column), in each of which there are two quarks (with electrical charge $\frac{2}{3}$ and $-\frac{1}{3}$) and two leptons (with electrical charge -1 and 0).

The bosons can also be further classified into vector and scalar bosons. The vector bosons are gauge bosons, i.e. they act as exchange particles of the fundamental interactions (gauge theories). The only known scalar boson is the Higgs-boson.

As a matter of fact, not all elementary particles take part in all of the fundamental forces. In the table below is shown, which of the fermions interact via which interaction.

	Interactions (exchange particle)		
Fermions	electromagnetic (photon)	strong (gluon)	weak ($W^{\pm}$, Z)
Quarks	×	×	×
e, μ, τ	×		×
ν_e, ν_μ, ν_τ			×

Since only quarks interact strongly, they are the main research objects to study the strong

interaction.

2.2 Quantum chromodynamics

The strong interaction is described by quantum chromodynamics (QCD). Similar to quantum electrodynamics (QED), which describes the interaction of electrically charged particles, there also exists a charge in QCD. This charge is called *colour charge*. There are three possible (anti-) colours the (anti-) quarks carry: (anti-) red, (anti-) green and (anti-) blue ($\bar{r}\bar{g}\bar{b}/rgb$). Gluons carry both a colour and an anti-colour hence there are eight possible gluons that act as exchange particles in QCD. Because of their colour charge gluons can also participate in the strong interaction.
An important property of QCD is *colour confinement* due to which only colour-neutral particles exist in nature. This can be realised in hadrons which consist of partons (quarks and gluons) that can be combined to achieve such a colour-neutral state. Hereby two possible types of hadrons can be created. On the one hand, a colour-neutral particle can be formed by a quark and an anti-quark ($q\bar{q}$). These hadrons are called *mesons*. The colour of the quark and the anti-colour of the anti-quark thereby cancel each other out ($r\bar{r}$, $g\bar{g}$, $b\bar{b}$). On the other hand, colour-neutrality can be achieved by combining all three (anti-) colours together thus a particle consisting of three (anti-) quarks is color-neutral ($\bar{q}\bar{q}\bar{q}$, qqq). Such particles are called *baryons*.
To further explain confinement, it is worth taking a look at the potential of the strong interaction:

$$V = -\frac{\alpha_s(r)}{r} + k \cdot r. \tag{2.1}$$

The first term of Eq. 2.1 dominates at small distances r with the coupling strength α_s and shows similar to the Coulomb potential of QED a $1/r$ dependence. Important for the confinement is the second term of the potential. It shows a linear increase for large distances meaning with growing distance there is an increase of energy in a system. If the system then has enough energy a $q\bar{q}$ pair is created which produces colour-neutral objects again. Therefore a parton can not be isolated and is confined.
Another interesting feature of QCD is the behavior of the coupling strength α_s. α_s as function of the squared momentum transfer Q^2 can be expressed as follows

$$\alpha_s(Q^2) = \frac{12\pi}{(33 - 2n_\mathrm{f}) \cdot \ln(Q^2/\Lambda^2_\mathrm{QCD})}, \tag{2.2}$$

where n_f is the number of quark-flavours involved and Λ_QCD is the scaling variable of QCD. As shown in Fig. 2.2 the coupling strength increases for decreasing Q.

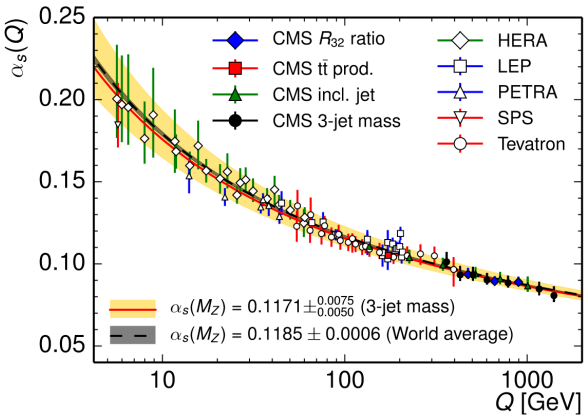

Figure 2.2: α_s as function of momentum transfer Q measured by different experiments [2].

Considering Heisenberg´s uncertainty principle which relates the momentum transfer to the distance of two particles ($Q \sim 1/r$) one can also relate the coupling strength to this distance. Hence it decreases with decreasing r. Under these circumstances, there is no confinement anymore and partons are able to act as free particles. Because α_s decreases asymptotically this property is called *asymptotic freedom*. The state of this deconfined matter is called the quark-gluon plasma (QGP) which can only be produced at high temperatures or densities.

2.3 Evolution of the QGP

These high temperatures and densities are only reached in ultra-relativistic heavy-ion collisions on Earth. Hereby the partons of the nuclei collide and produce a hot and dense medium which expands and cools down with time.
In Fig. 2.3 the phase diagram of QCD is shown. Heavy-ion collisions happening at the Large Hadron Collider (LHC) at CERN are located at low baryon densities but high temperatures thus in the region where a crossover between the two phases of matter happens.

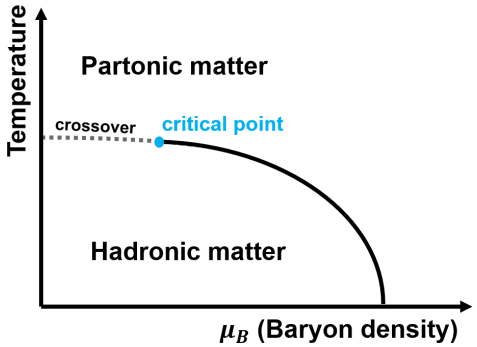

Figure 2.3: Sketch of the QCD phase diagram. The partonic matter represents the deconfined state (QGP). The crossing between hadronic and partonic matter is up to the critical point of a first-order phase transition. If the critical point is reached there happens a crossover.

The partonic matter created in the collision expands and cools down until it reaches the *critical temperature* T_C ($\sim 170\,\text{MeV}$). At this temperature, the partons are starting to form

hadrons again and a hot hadronic matter is created. The hadronic matter cools further down and reaches the *chemical freezeout*. Hereby the particle composition of the hadronic matter is defined. After cooling down and expanding even more a *kinetic freezout* happens meaning the particles are not interacting with each other anymore and start to move freely.
To examine the QGP and its properties, particles that are created in the partonic matter and pass the hadronic matter without any strong interaction are needed. Probes that fulfill all of these conditions are dileptons and photons.

2.4 Dileptons

Dileptons are correlated lepton pairs that are produced in every stage of the collision. They do not interact strongly and are therefore excellent messengers of the QGP.
The same applies to photons. They can be produced in the partonic matter via various processes, some examples are shown in Fig. 2.4.

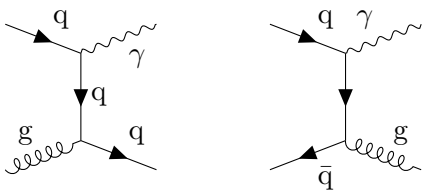

Figure 2.4: Photon production in partonic matter via Compton scattering (left) or quark-antiquark annihilation (right) [3].

In the hadronic matter vector mesons (ρ^0, π^+, π^-) are the dominant constituents producing photons (Fig. 2.5).

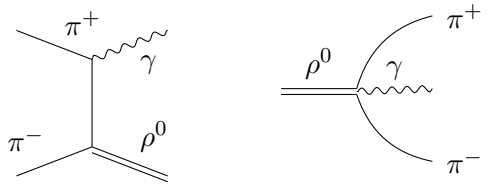

Figure 2.5: Examples for photon production processes in hadronic matter via $\pi^+\pi^-$ annihilation (left) or the decay of a ρ^0-meson (right) [3].

Interestingly the photon and dilepton production are connected. In all processes real photons are produced, a similar process with virtual photons exists [4]. Virtual photons (γ^*) carry a mass and can therefore decay into massive particles, e.g. dileptons. This *invariant mass m* is, as the *transverse momentum* p_T, a fundamental quantity for characterising dileptons.
By comparing the thermal photon and dilepton production rate the relation between both is becoming more obvious. The real photon production rate can be defined as follows

$$k^0 \frac{\mathrm{d}R}{\mathrm{d}^3\boldsymbol{k}} = -\frac{\alpha}{\pi^2}\mathrm{Im}\Pi^\mathrm{T}_\mathrm{em}(M=0, k, T) f^\mathcal{B}(k^0, T), \tag{2.3}$$

whereas the dilepton production rate is defined as

$$\frac{\mathrm{d}R}{\mathrm{d}^4k} = -\frac{\alpha^2}{3\pi^3}\frac{L(M)}{M^2}\mathrm{Im}\Pi^{\mu}_{\mathrm{em},\mu}(M,k,T)f^B(k^0,T), \tag{2.4}$$

where α is the electromagnetic coupling strength, M the mass of the virtual photon or the dilepton, k denotes a four-dimensional vector consisting of the energy (k^0) and the momentum ($\boldsymbol{k}$), $f^B(k^0,T)$ denotes the Boltzmann factor

$$f^B(k^0,T) = 1/(e^{\beta k^0/T}-1), \tag{2.5}$$

$\frac{\alpha}{3\pi}L(M)/M^2$ is a factor describing the decay of virtual photons into dileptons with

$$L(M) = \sqrt{1-\frac{4(m_\mathrm{e})^2}{M^2}}(1+\frac{2(m_\mathrm{e})^2}{M^2}), \tag{2.6}$$

m_e is the mass of an electron [5]. As can be seen, the dilepton production rate directly relates to the photon production rate. A rather complicated but important function the production rates depend on is the *spectral function* $\mathrm{Im}\Pi^{\mu}_{\mathrm{em},\nu}(k)$ (McLerran-Toimela relation [6]). The spectral function has a longitudinal and a transverse component, $\mathrm{Im}\Pi^{\mathrm{L}}_{\mathrm{em}}(k)$ and $\mathrm{Im}\Pi^{\mathrm{T}}_{\mathrm{em}}(k)$. The transverse component is the only component important for real photons because the longitudinal part of the spectral function vanishes for $M \to 0$. The spectral function and its importance in describing interactions of particles with a medium will be further explained in the following.

2.4.1 Spectral function

The movement of electrically charged particles can be described as currents. Since there are particles in the partonic and hadronic matter which carry electrical charges there are also currents that flow through both media. An important quantity to depict the development of these currents over time is the *current-current correlator*[1]

$$\tilde{\Pi}^{\mu\nu}_{em}(k) = i\int \mathrm{d}^4x e^{ikx}\Theta(x^0)\langle[\boldsymbol{J}^{\mu}_{\mathrm{em}}(x),\boldsymbol{J}^{\nu}_{\mathrm{em}}(0)]\rangle, \tag{2.7}$$

where $\Theta(x^0)$ is the Heaviside-function [9], $\boldsymbol{J}^{\nu}_{\mathrm{em}}(0)$ denotes an initial current and $\boldsymbol{J}^{\mu}_{\mathrm{em}}(x)$ denotes this current after some time [7]. A way to further simplify and actually calculate Eq. 2.7 is via the spectral function $\mathrm{Im}\tilde{\Pi}^{\mu\nu}_{\mathrm{em}}(k)$ or more accurately the *photon self-energy*. This self-energy arises from self-interaction meaning a photon interacts with its surroundings which results in the photon gaining energy (effective mass)[2]. Therefore the self-energy (and thus the current-current correlator) contains all information about a particle´s interaction with a

[1] Note that the correlator shown here is actually the *retarded Fourier-transformed* electromagnetic current-current correlator [7, 8].

[2] Photons can get an effective mass and still be quasi-real since this mass is the result of the interaction with a medium.

medium. Considering photons are produced in the partonic and hadronic matter this energy carries valuable information about both.
Depending on the phase of the medium there are different approaches to calculate the photon self-energy. In partonic matter it can be calculated via the hard-thermal loop (HTL) formalism [10]. In a hard thermal loop, a virtual photon produces a $q\bar{q}$ pair which then annihilates itself by emitting a virtual photon again.
Since the hadronic electromagnetic currents in the hadronic matter are dominated by vector mesons the photon self-energy[3] is calculated within the vector meson dominance model (VDM) [11]. An example for the VDM is shown in 2.6 where a ρ^0-meson produces a $\pi^+\pi^-$ pair which annihilates itself by creating a ρ^0-meson again.

Figure 2.6: Diagram of a hard-thermal loop (left) and of the VDM (right).

With the spectral function, the dilepton and photon production rate can be calculated as well as the currents of the media via the current-current correlator.
One property still unknown connected to these currents and related to the spectral function is the electrical conductivity.

2.4.2 Electrical conductivity

The *electrical conductivity* σ_{el} is a fundamental property of matter and describes the ability to transport charges through it. This transport coefficient is defined by Ohm's law

$$\langle eJ^i_{\mathrm{em}} \rangle = \sigma_{\mathrm{el}} \langle E \rangle, \tag{2.8}$$

with J^i_{em} being the current, e the elementary charge and E being an electric field [12]. Hence, the electrical conductivity describes how well charged particles flow if induced by an electric field, and it, therefore, determines how strong the current will be and how long it will last in a medium. Likewise, the currents in the partonic and hadronic matter depend on σ_{el}. So far there are many theoretical predictions for σ_{el}, such as lattice calculations or transport models (e.g. BAMPS), but they all vary largely, as shown in Fig. 2.7.

[3] Actually the ρ self-energy is calculated in the VDM, however, ρ-mesons can change into photons, therefore it does not make a difference (go to 2.5 and 2.6) [11].

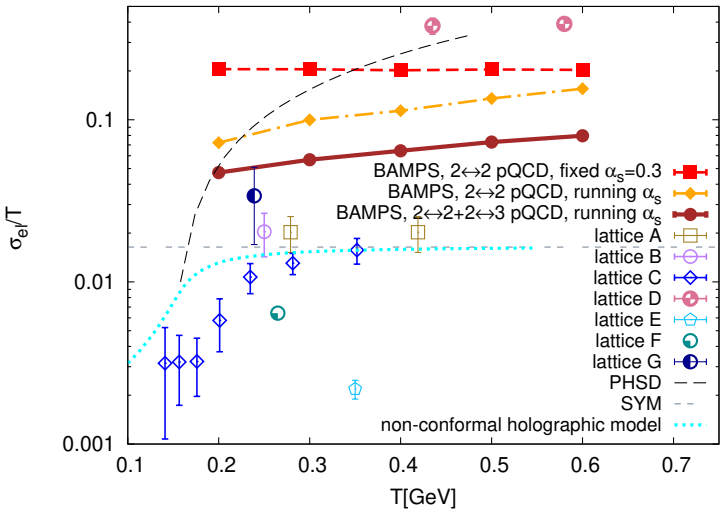

Figure 2.7: Different theoretical predictions for the electrical conductivity of partonic and hadronic matter [13].

The Green-Kubo relation shows how σ_{el} and the spectral function are connected[4]

$$\sigma_{\mathrm{el}} = \frac{1}{3} \lim_{k^0 \to 0} g_{\mu\nu} \frac{\mathrm{Im}\tilde{\Pi}^{\mu\nu}_{\mathrm{em}}(k^0, \mathbf{0})}{k^0}. \tag{2.9}$$

If one could measure the spectral function at energy $k^0/T \backsim 0$ (Fig. 2.8), one would get the value of σ_{el} for the hot deconfined matter. This value also depends on the coupling strength α_s.

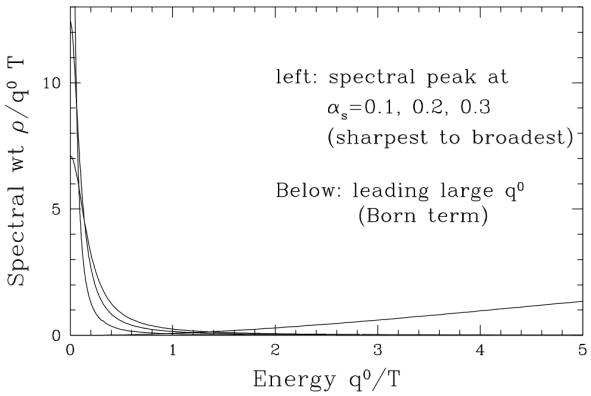

Figure 2.8: Spectral function (here ρ) for different coupling strengths α_s. Electrical conductivity is the intercept point at the y-axis (energy $q^0 = 0$ equivalent to $k^0 = 0$) [12].

The spectral function plays a role in the dilepton and photon production and is therefore part of the photon and dilepton yield (in this work we examine the dielectron yield). If the signal of the spectral function could be extracted out of the dielectron yield at low dielectron mass m_{ee} the value of the electrical conductivity could be constrained.

[4] For a full derivation refer to [12] and [14].

2.4.3 Direct dielectrons

A direct signal from direct dielectrons from the QGP and the hadronic matter arises as thermal radiation. Hereby direct dielectrons are produced in processes such as quark-antiquark annihilation or $\pi^+\pi^-$ annihilation (Fig. 2.4 and 2.5). Out of the invariant mass spectrum of these thermal dielectrons, the mean temperature of the produced medium can be extracted as well as the spectral function and therefore the signal of the electrical conductivity. Hence, the thermal signal is the signal that one wants to detect.
There are other processes that produce direct dielectrons but do not necessarily transport information about the media. One process like this is the Drell-Yan process. During the collision quarks from one nucleus and antiquarks from the other can annihilate themselves by emitting virtual photons (dielectrons). Since the nuclei collide with a high energy the dielectrons produced carry a high invariant mass.
Dielectrons that do not carry information about the produced matter are considered background. A rather large background arises from the decays of hadrons that are produced in the hadronic matter.

2.4.4 Hadronic background

The hadronic background can be divided into three different dielectron mass (m_{ee}) regions. The low invariant mass region (LMR, $m_{\mathrm{ee}} < 1.1\,\mathrm{GeV}/c^2$) of the dielectron mass spectrum is dominated by dielectrons produced in the decay of *light-flavour* hadrons. Light-flavour hadrons consist of the three lightest quarks (up, down, strange) and are produced late in the hadronic phase. Resonance peaks in the spectrum arise from two-body-decays (ρ, ϕ, $\omega \rightarrow e^-\ e^+$) of light-flavour hadrons. Another important decay is the Dalitz-decay (three-body-decay) where π^0, η, η‘, ω and ϕ decay into an electrically neutral particle (e.g. photon) and a dielectron.
In the intermediate mass region (IMR, $1.1\,\mathrm{GeV}/c^2 < m_{\mathrm{ee}} < 2.7\,\mathrm{GeV}/c^2$) dielectrons from decaying *open heavy-flavour* hadrons are found. Open heavy-flavour hadrons consist of charm- or beauty quarks and light quarks.
Dielectrons from the decay of heavier hadrons (e.g. J/Ψ) are dominant in the high mass region (HMR, $m_{\mathrm{ee}} > 2.7\,\mathrm{GeV}/c^2$). Also, dielectrons from the Drell-Yan process are located in the HMR.
In addition to the hadronic background, there is also the electromagnetic background.

2.4.5 Electromagnetic background

The electromagnetic background originates from the interaction of the Lorenz-contracted electromagnetic fields produced by the colliding nuclei. Hereby a flux of quasi-real photons arises and photons originating from the field of one nucleus interact with photons originating from the field of the other nucleus and produce dielectrons (Fig. 2.9). One can differentiate between two possible interactions depending on the impact parameter. For

ultra-peripheral collisions (UPCs) the impact parameter between the two nuclei is larger than 2 R_{A} (R_{A}=nuclear radius). In UPCs the colliding nuclei do not interact hadronically but only through two-photon or photonuclear interaction.
For *hadronic overlaps (HOs)* the impact parameter is smaller than 2 R_{A}. Hadronic collisions can occur in the case of HOs, at the same time, the quasi-real photons from the fields of the nuclei can still interact and produce dielectrons.

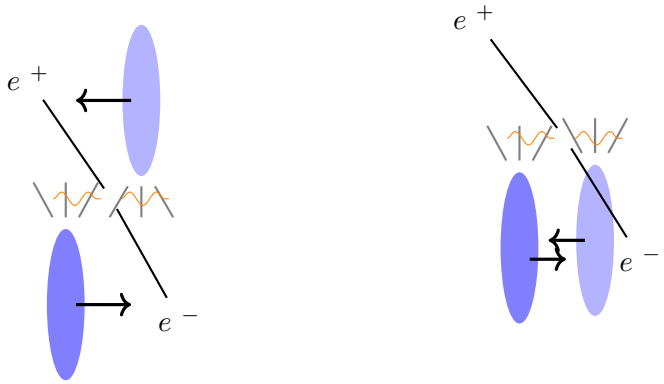

Figure 2.9: Sketch of ultra-peripheral collisions (UPCs) (left) and hadronic overlaps (HOs) (right). The nuclei (blue) are Lorentz-contracted as well as the electromagnetic fields (gray lines on the ends of the nuclei). The electromagnetic fields interact via photons (orange) and produce a dielectron.

The produced dielectrons originate from quasi-real photons with momenta predominantly in the beam direction. Hence, the resulting dielectrons are characterised by very small pair transverse momentum ($p_{\mathrm{T,ee}} < 0.3\,\mathrm{GeV}/c$).
The electromagnetic background is a relevant factor to consider in heavy-ion collisions because the flux of the quasi-real photons produced is proportional to Z^2 (Z = charge number, 1 for a proton, 82 for lead (Pb)) and is, therefore, larger for heavy-nuclei.

3 ALICE 3

ALICE (**A** **L**arge **I**on **C**ollider **E**xperiment) is one of the four big experiments at the LHC at CERN. It investigates the partonic matter produced in relativistic heavy-ion collisions. Planned for the mid-2030s is a new setup for ALICE, ALICE 3. The detector will continue measuring and observing the properties of the deconfined matter produced in heavy-ion collisions. Furthermore, there are many other physics motivations, e.g. chiral symmetry restoration which would lead to a modified dilepton spectrum in the light vector meson mass range [15].
ALICE 3 is scheduled to be build during the long shutdown 4 of the LHC, inside the L3 magnet yoke currently used as a magnet for ALICE, and will consist of several different detectors, placed inside a superconducting magnet system, as shown in 3.1.

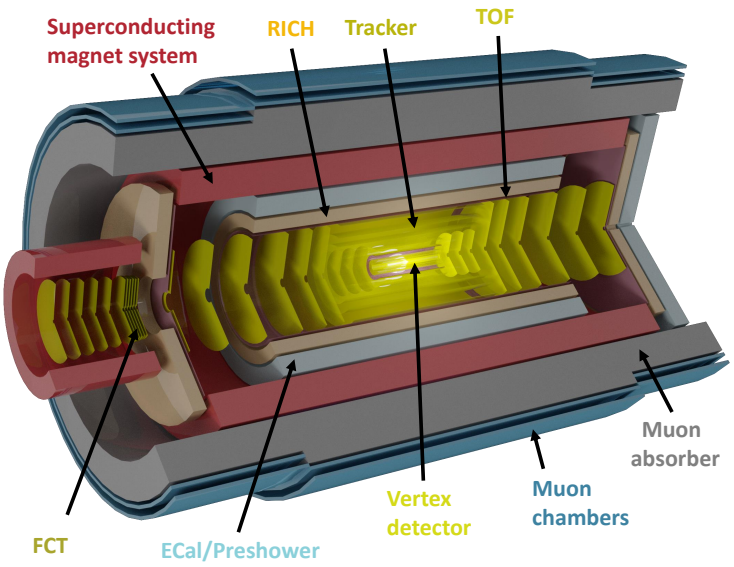

Figure 3.1: Possible setup for ALICE 3. Important for identifying dielectrons are the Ring Imaging Cherenkov (RICH) and Time of flight (TOF) detectors [15].

Very close to the interaction point sits the silicon vertex tracker which provides a wide rapidity acceptance over a broad p_{T} range. To provide the necessary pointing resolution (ability to determine the trajectory of particles), the tracking should start as close to the interaction point as possible. Therefore, part of the vertex tracker is considered to be installed inside the beam pipe of the LHC.
Important for the measurement and identification of dielectrons are the **R**ing **I**maging **Ch**erenkov (RICH) detector and the **T**ime **o**f **F**light (TOF) system. ALICE 3 is considered to measure dielectrons in a $p_{\mathrm{T,ee}}$ range from 0.05 GeV/c up to 3 GeV/c and in a mass range from 0.05 GeV/c^2 to 4 GeV/c^2. However, these values also depend on the magnetic field used in the experimental setup.

3.1 Magnetic field

A magnetic field curves the tracks of charged particles flying through the detectors and based on that, the transverse momentum can be calculated. The transverse momentum is important for particle identification (PID) because one can either calculate the mass with the momentum and the measured velocity (TOF) or plot the different measurable quantities of the detectors (e.g. velocity v/c for the TOF, Cherenkov angle θ for the RICH) vs the momentum (Fig. 3.4 and 3.5) and can identify the different particles from these plots. PID also depends on the strength of the magnetic field because if the magnetic field is too strong or too weak the particles either curve so much that they do not even reach some detectors or they do not curve enough and it is not possible to distinctively calculate the transverse momentum. Therefore, different strengths of the magnetic field and their influence on the performance of the different detectors are investigated. In the figure below is the RICH and TOF PID performance shown for magnetic fields of $B = 0.5$ T and $B = 2$ T.

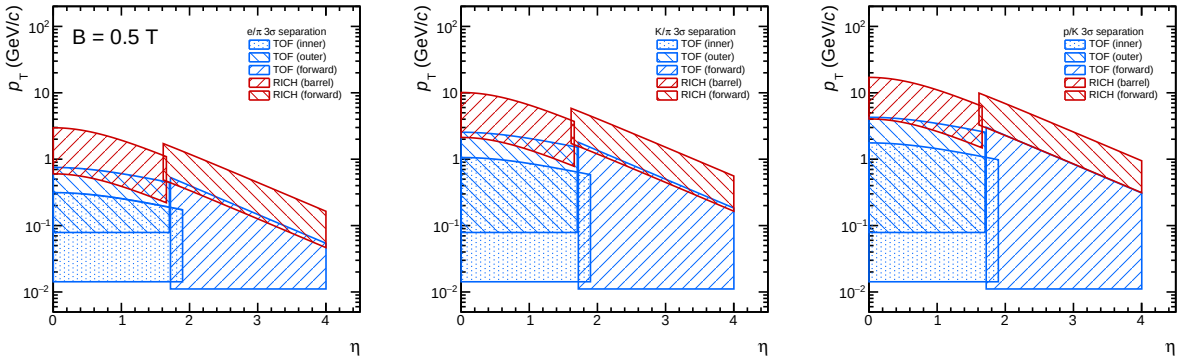

Figure 3.2: PID (e = electron, π = pion, K = Kaon, p = proton) over different p_{T} and η regions with a magnetic field of $B = 0.5$ T (RICH [red] and TOF [blue]). The studies of the magnetic fields were done with a pseudorapidity $|\eta| < 4$. The different plots show the ability to separate e/π, K/π, and p/K within a 3σ surrounding [15].

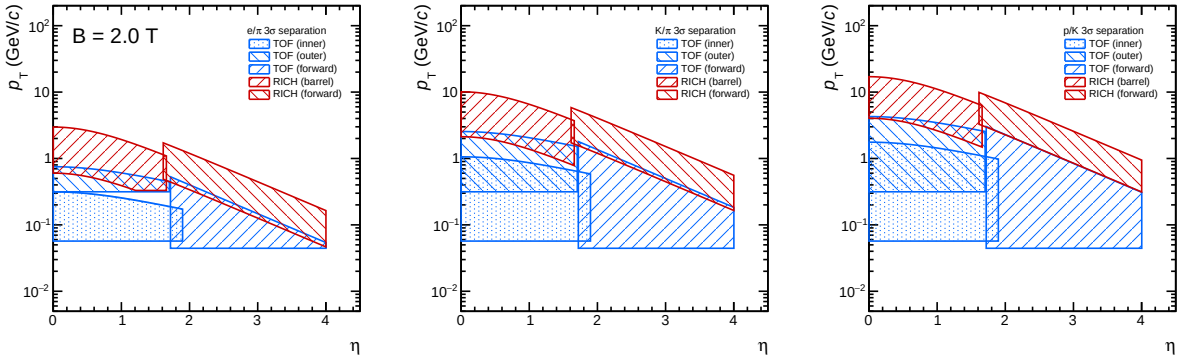

Figure 3.3: PID over different p_{T} and η regions with a magnetic field of $B = 2$ T (RICH [red] and TOF [blue]) [15].

As can be seen in Fig. 3.2 and 3.3 a magnetic field of 0.5 T ensures a PID over a larger p_{T} region than the 2 T field[5]. It is therefore considered to have dedicated data-taking periods (runs) with a reduced magnetic field of the superconducting magnet in Run 5 or 6 to reach low p_{T} for measurements e.g. of low-mass dielectrons [15].

3.2 TOF system

The TOF system measures the time of flight of the particles (the time the particles take from the interaction point to the TOF layers). By using that measured time and the length of the particle's track the velocity can be calculated. With the momentum, one can determine the mass of the particle.

ALICE 3 is considered to have inner and outer TOF layers located at 20 cm and 105 cm from the beam pipe and also forward disks on both sides of the experiment located at 405 cm from the interaction point [15].

In Fig. 3.4 the velocity (v/c) vs the momentum is plotted. For this study, a Pb-Pb collision with $\sqrt{s_{\mathrm{NN}}}$ = 5.52 TeV was simulated. The study was performed for a pseudorapidity $|\eta| < 1.44$, i.e. using the TOF detectors in this bound, and a magnetic field $B = 2$ T.

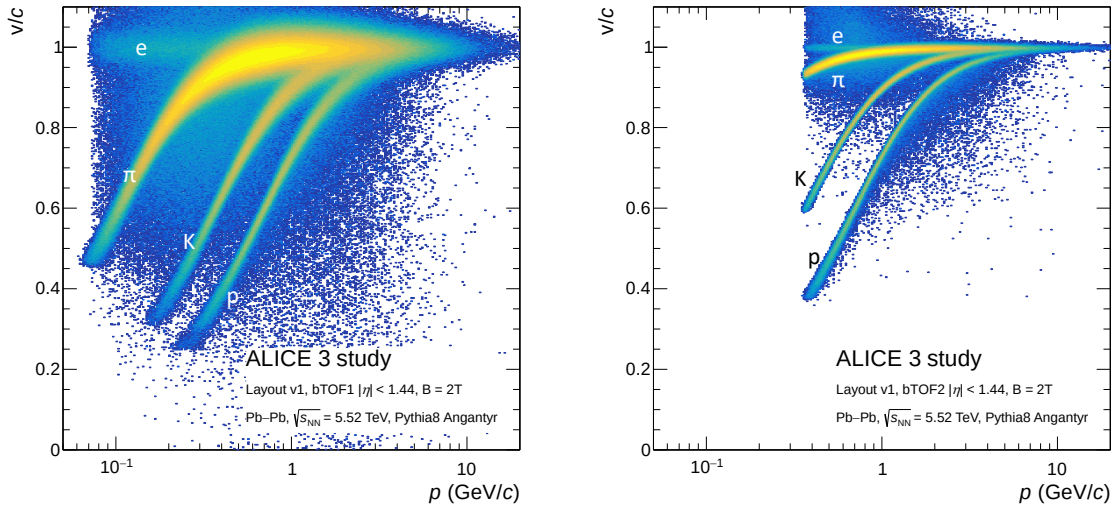

Figure 3.4: PID via measurement of the momentum and the velocity (v/c) by the inner TOF (left) and the outer TOF (right) with a magnetic field of $B = 2$ T. A Pb-Pb collision with $\sqrt{s_{\mathrm{NN}}} = 5.52$ TeV was simulated. The study was performed for a pseudorapidity $|\eta| < 1.44$ and a magnetic field $B = 2$ T [15].

The minimum $p_{\mathrm{T,min}}$ a particle has to have to reach a detector layer at a given radius R from the beam axis can be calculated via the following equation

$$p_{\mathrm{T}}\,[\mathrm{GeV}/c] = 0.3 \cdot q \cdot B\,[\mathrm{T}] \cdot \frac{R}{2}\,[\mathrm{m}], \tag{3.1}$$

[5] Interactions of particles with the detector material are not yet included in these graphics [15].

with q being the charge of the particle, B is the magnetic field applied. To calculate the minimum $p_{\mathrm{T,min}}$ of the TOF, one needs $R_{\mathrm{TOF,layer}}$. For an electron, the minimum transverse momentum to reach the inner TOF, with $R_{\mathrm{TOF,layer}} = 0.2\,m$ and $B = 2\,\mathrm{T}$, is $p_{\mathrm{T,min}} = 0.06\,\mathrm{GeV}/c$. The minimum $p_{\mathrm{T,min}}$ an electron has to have to reach the outer TOF, with $R_{\mathrm{TOF,layer}} = 1.05\,m$ and $B = 2\,\mathrm{T}$, is $p_{\mathrm{T,min}} = 0.315\,\mathrm{GeV}/c$.
The inner TOF can identify particles down to low p_{T}, which provides a clear separation between electrons and pions because it is closer to the interaction point than the outer TOF. The separation power between different particles is proportional to the length of the track divided by the intrinsic timing resolution of the TOF (σ_{TOF}=20 ps), hence, the outer TOF shows better accuracy at measuring pions, Kaons, and protons, especially at higher p_{T}.
Identifying and separating electrons and pions further at higher p_{T} (up to 2 GeV/c) can be achieved with the RICH detector.

3.3 RICH detector

RICH detectors are based on the *Cherenkov effect*. The Cherenkov effect describes the emission of electromagnetic radiation when a charged particle enters a medium with a velocity larger than the phase velocity of light in that medium. The emission angle θ (Cherenkov angle) under which the radiation is emitted depends on the refraction index of the medium n and the ratio of the speed of light c and the velocity of the particle traveling through that medium v

$$cos(\theta) = \frac{c}{nv}. \tag{3.2}$$

Detectors built to detect Cherenkov radiation consist of a liquid or gas, also called radiator material. Photomultipliers are mostly used to detect the emitted photons.
In RICH detectors all photons emitted under the same angle can be seen as a ring in the detector. Hence, the angle (and thus the velocity) can be extracted from just the sizes of the rings. To identify the different particles, one can plot the Cherenkov angle vs the momentum, as shown in Fig. 3.5. The study was performed for the same magnetic field B (= 2 T) and η range ($|\eta| < 1.44$) as for the TOF detector.

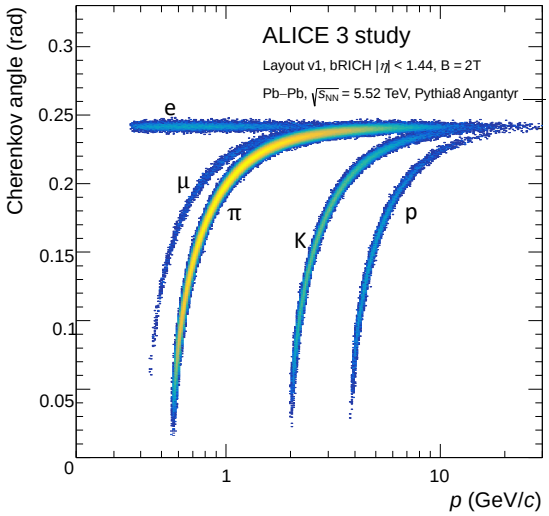

Figure 3.5: PID via measurement of the momentum and the Cherenkov angle with a magnetic field of $B = 2$ T. For this study also a Pb-Pb collision $\sqrt{s_{\mathrm{NN}}} = 5.52$ TeV was simulated and conducted with a pseudorapidity $|\eta| < 1.44$ and a magnetic field $B = 2$ T [15].

The particles need to have a minimum p_{T} ($p_{\mathrm{T,min}}$) to reach the RICH detector. In addition, they have to have a velocity larger than c/n to emit Cherenkov radiation. This can be translated into a minimum p_{T} ($p_{\mathrm{T,min,Cherenkov}}$), increasing proportionally to the mass of the particle, to emit a signal. For electrons, the minimum momentum is smaller than for the other particles, because they are lighter ($p_{\mathrm{T,min,Cherenkov}} = 0.002\,\mathrm{GeV}/c$ with aerogel as radiator material) which is also why they emit Cherenkov radiation under a large angle even at low momentum. The RICH considered for ALICE 3 could separate electrons and pions up to $2\,\mathrm{GeV}/c$ and has an angle resolution of 1.5 mrad.
Also important is the medium with which the detector is filled because the higher the speed of light is in that medium the lighter the particles have to be to emit Cherenkov radiation for a given momentum. Hence, particle identification also depends on the radiator material used in the detector. Aerogel is considered as radiator material for the RICH in ALICE 3 [15]. It has a refraction index of $n = 1.03$ and therefore ensures a continuous particle identification beyond the TOF (as seen in Fig. 3.2).

4 Analysis

All various contributions contributing to the overall dielectron yield are investigated more closely in the following before they are compared in section 4.5.

4.1 Expected thermal signal

The expected thermal signal containing information about the electrical conductivity is not coming from just the partonic matter, but rather a combined signal from partonic and hadronic matter. Ralf Rapp calculated the different thermal signals produced at mid-rapidity ($|y_{\mathrm{ee}}| = 0$) for a Pb-Pb collision at $\sqrt{s_{\mathrm{NN}}} = 5.02$ TeV for the partonic matter and for the hadronic matter [16, 17]. Used here are two different assumptions about the hadronic matter and hence, two different values for the electrical conductivity. If pions from the hadronic matter scatter on other pions ($\pi\pi$-Bremsstrahlung) they interact electromagnetically and produce dielectrons. Since they are the dominant contribution in the hadronic matter, they therefore significantly change the thermal dielectron yield. In Fig. 4.1 are the three different thermal dielectron yields from the partonic matter (QGP), the hadronic matter with ($\mathrm{HM}_{\pi\pi}$) and without (HM) $\pi\pi$-Bremsstrahlung shown.

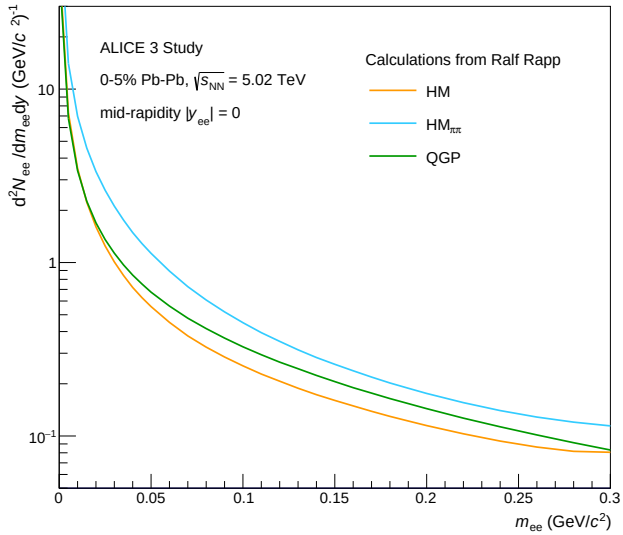

Figure 4.1: Different calculations for the expected thermal signal in the dielectron yield: QGP (green) and hadronic matter with ($\mathrm{HM}_{\pi\pi}$) and without (HM) $\pi\pi$-Bremsstrahlung (yellow and blue). The thermal signal at mid-rapidity ($|y_{\mathrm{ee}}| = 0$) was calculated for a Pb-Pb collision at $\sqrt{s_{\mathrm{NN}}} = 5.02$ TeV [16, 17].

The difference between a signal coming from hadronic matter with $\pi\pi$-Bremsstrahlung or hadronic matter without it has to be large enough to be detectable and to accurately extract the signal for the QGP. A way to enhance that difference is to go to low $p_{\mathrm{T,ee}}$.

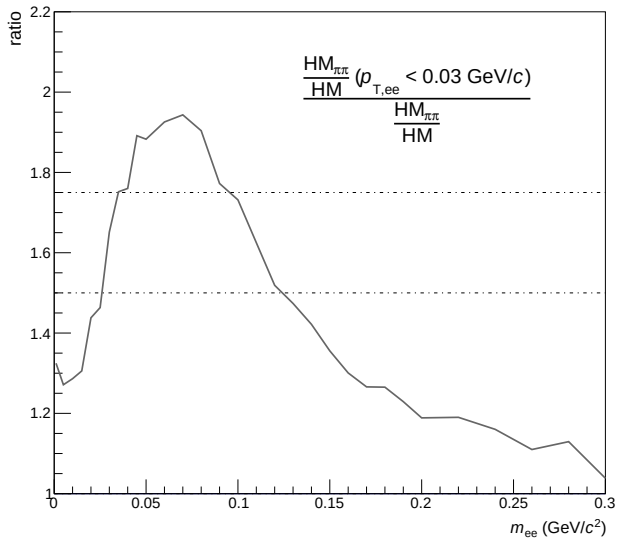

Figure 4.2: Double ratio of thermal radiation from the hadronic matter with and without $\pi\pi$-Bremsstrahlung and a $p_{\mathrm{T,ee}}$ cut ($p_{\mathrm{T,ee}} < 0.03\,\mathrm{GeV}/c$) [16, 17].

As can be seen in Fig. 4.2 at low $p_{\mathrm{T,ee}}$ one can better differentiate between the hadronic matter with and without $\pi\pi$-Bremsstrahlung, which suggests measuring the dielectron yield at low $p_{\mathrm{T,ee}}$ in the mass region $0.05\,\mathrm{GeV}/c^2 < m_{\mathrm{ee}} < 0.14\,\mathrm{GeV}/c^2$, where the yield would be the most sensitive to σ_{el}.

4.2 Expected hadronic background

The hadronic background is estimated by tuning Monte Carlo simulations to describe measured hadron spectra. The p_{T}-differential yields of the different hadrons were parameterised and extrapolated to $p_{\mathrm{T}} = 0$ to be taken as input for a fast Monte Carlo simulation.
The π^0 parametrisation was based on the measurement of charged pions ($\pi^{\pm}$) down to $p_{\mathrm{T,ee}} = 0.1\,\mathrm{GeV}/c$ in 0-5 % central Pb-Pb collisions [18] with a correction for the differences due to isospin-violating decays between π^0 and $\pi^{\pm}$ [19].
The η parametrisation is based on the η/π^0 ratio being the mean value of the η/π^0 ratio in p-p collisions at 5.02 TeV and the $K^{\pm}/\pi^{\pm}$ ratio measured in Pb-Pb collisions at 5.02 TeV.
The remaining light-flavoured hadron ($\omega, \rho, \phi, \eta'$) parametrisations were based on m_{T} scaling. m_{T} is the transverse mass and can be calculated via $m_{\mathrm{T}} = \sqrt{m^2 + {p_{\mathrm{T}}}^2}$. Basing the parametrisation on m_{T} scaling means that all the spectra of the light mesons as a function of m_{T} are the same and just differ by a normalisation factor.
The hadronic background produced at mid-rapidity $|y_{\mathrm{ee}}| < 0.5$ was further simulated with no fiducial cuts. In Fig. 4.3 are the dielectrons from the different hadrons contributing to the hadronic background shown. The sum of all those contributions is the hadronic Cocktail (hadr. Cocktail).

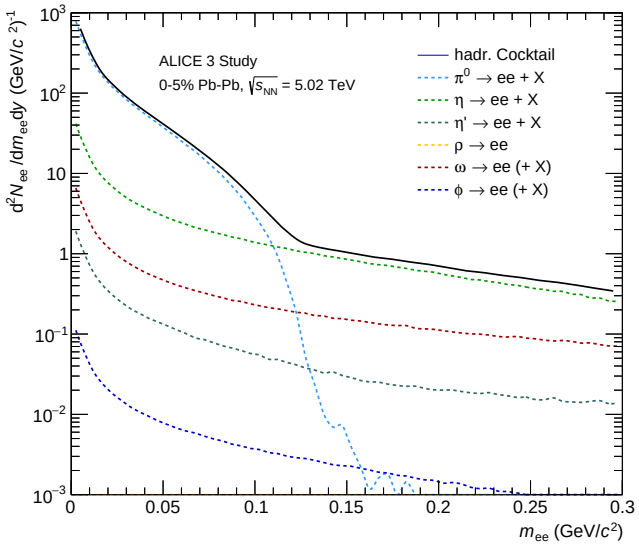

Figure 4.3: Hadronic Cocktail (hadr. Cocktail, black line) for a Pb-Pb collision with 0-5 % centrality at $\sqrt{s_{\mathrm{NN}}} = 5.02$ TeV with the contributions of the different hadrons. As can be seen, the most dominant contributions are coming from the Dalitz decay ($\pi^0, \eta, \eta', \omega, \phi \rightarrow e^+e^- + X$).

At low m_{ee}, dielectrons from the Dalitz decay of the π^0-meson dominate the spectrum, hence in the low mass range, one does not expect to detect a contribution of the thermal signal. One is more likely to be sensitive to the thermal signal after the dropping of the π^0 contribution at $m_{\mathrm{ee}} \approx 140\,\mathrm{MeV}/c^2$.
A precise description with good statistics for the hadronic background is needed to evaluate the possibility of detecting a thermal signal accurately.

4.3 Expected electromagnetic background

The electromagnetic backgrounds were simulated with the event generator STARlight.

4.3.1 STARlight

STARlight was developed in the late 1990s [20]. The program generates events via Monte Carlo simulations and calculates cross-sections for a variety of two-photon or photonuclear interactions. In the two-photon interaction, the electromagnetic fields of the nuclei collide and couple to particles that carry electric charges allowing for a variety of different final states. The fields are hereby described by the Weizsäcker-Williams method as a flux of quasi-real photons [21]. The photon flux for ultra-peripheral collisions (UPC) is calculated as follows

$$\frac{\mathrm{d}^2 N_{\gamma\gamma}(k_1, k_2)}{\mathrm{d}k_1 \mathrm{d}k_2} = \int\int \mathrm{d}^2 b_1 \mathrm{d}^2 b_2 P_{\mathrm{NOHAD}}(|\tilde{b_1} - \tilde{b_2}|) N(k_1, \tilde{b_1}) N(k_2, \tilde{b_2}), \tag{4.1}$$

where k_1 and k_2 are energies of the two photons, $\vec{b_1}$ and $\vec{b_2}$ are the positions of the photons from the nuclei, $N(k_1, \vec{b_1})$ and $N(k_2, \vec{b_2})$ are the corresponding photon densities of both colliding nuclei and P_{NOHAD} denotes the probability of having no hadronic interaction at given impact parameter ($|\vec{b_1} - \vec{b_2}|$). For nucleus-nucleus collisions (e.g. Pb-Pb) P_{NOHAD} is calculated as follows

$$P_{\mathrm{NOHAD}}(\vec{b}) = e^{-\sigma_{\mathrm{NN}} T_{\mathrm{AA}}(\vec{b})}, \tag{4.2}$$

with σ_{NN} as nucleon-nucleon interaction cross-section and T_{AA} as nuclear overlap function. The nuclear overlap function is calculated from nuclear density profiles which are assumed to follow a Woods-Saxon distribution [21].
To calculate the total cross-section of two-photon interaction to produce a final state X

$$\sigma = \int\int \frac{\mathrm{d}^2 N_{\gamma\gamma}}{\mathrm{d}\,W \mathrm{d}\,Y} \sigma(\gamma_1\gamma_2 \to \mathrm{X}) \mathrm{d}\,Y \mathrm{d}\,W, \tag{4.3}$$

one needs the final state invariant mass

$$W = \sqrt{4 k_1 k_2}, \tag{4.4}$$

the final state rapidity

$$Y = 0.5 \ln(\frac{k_1}{k_2}), \tag{4.5}$$

the two-photon luminosity $\mathrm{d}^2 N_{\gamma\gamma}/\mathrm{d}\,W \mathrm{d}\,Y$ and the two-photon cross-section $\sigma(\gamma_1\gamma_2 \to \mathrm{X})$. Eq. 4.3 becomes

$$\frac{\mathrm{d}^2\sigma}{\mathrm{d}\,W \mathrm{d}\,Y} = \frac{\mathrm{d}^2 N_{\gamma\gamma}}{\mathrm{d}\,W \mathrm{d}\,Y} \sigma(\gamma_1\gamma_2 \to \mathrm{X}) \tag{4.6}$$

in differential form.
Lepton pairs are created in STARlight via the equivalent photon approximation (EPA) approach in which the photons are considered to be massless. The cross-section for producing leptons via two-photon interaction is calculated by the Breit-Wheeler formula

$$\sigma(\gamma\gamma \to l^+ l^-) = \frac{4\pi\alpha^2}{W^2}[(2 + \frac{8m^2}{W^2} - \frac{16m^4}{W^4}) \ln(\frac{W + \sqrt{W^2 - 4m^2}}{2m}) - \sqrt{1 - \frac{4m^2}{W^2}}(1 + \frac{4m^2}{W^2})], \tag{4.7}$$

which is also used to calculate the shape of the mass distribution of the lepton pairs.
STARlight runs in two phases, while it calculates the cross-section in the first phase, it generates events in the second phase.
There are many parameters user settable such as the maximum and minimum $\gamma\gamma$ center of mass energy (W, equivalent to m_{ee}) and the number of bins in W, the Lorentz boost for both beams ($\sqrt{s_{\mathrm{NN}}}$), the charge of the beam projectiles and their atomic numbers (82 and 208 for Pb), the maximum pair rapidity ($|y_{\mathrm{ee}}|$) and the number of bins in y, also cuts on the single electron transverse momentum ($p_{\mathrm{T,e}}$) or the pseudorapidity (η). Furthermore, the number of events (N, one produced dielectron corresponds to one event) as well as the break-up mode are settable. The break-up mode determines how the nuclear break-up is handled, option 5

describes a non-hadronic break-up with an impact parameter greater than the sum of the nuclear radii (UPC). For the break-up mode 8, the condition of not having any hadronic collision is removed, i.e. the suppression factor P_{NOHAD}, although the hadronic collision is not simulated in itself. The impact parameter range between the two nuclei can also be set. If cuts are used on η and $p_{\mathrm{T,e}}$, STARlight calculates the total cross-section σ_{total} and the fiducial cross-section $\sigma_{\mathrm{fiducial}}$. The fiducial cross-section shows how many events are within those selections. To compare how much is cut away by using selections, events from UPCs were generated with STARlight with different restrictions in η and $p_{\mathrm{T,e}}$ but a wide range in pair rapidity.

$p_{\mathrm{T,e}}$ (GeV/c)	none	$0.2 \leqslant p_{\mathrm{T,e}} \leqslant 10$	none	$0.2 \leqslant p_{\mathrm{T,e}} \leqslant 10$	$0.2 \leqslant p_{\mathrm{T,e}} \leqslant 2$
η	none	none	$\lvert\eta\rvert < 0.8$	$\lvert\eta\rvert < 0.8$	$\lvert\eta\rvert < 0.4$
σ_{total} (b)	3.789	3.789	3.789	3.789	3.789
$\sigma_{\mathrm{fiducial}}$	3.789 b	281.313 mb	27.563 mb	23.535 mb	6.01 mb

As can be seen in the table, the stronger the selection in $p_{\mathrm{T,e}}$ and η the smaller the fiducial cross-section. For the last selection, 99.84 % of the generated events are rejected.
Finally, 100,000 events per UPCs and hadronic overlaps (HOs) were simulated in the mass region $0.002\ \mathrm{GeV}/c^2 \leq m_{\mathrm{ee}} \leq 0.3\ \mathrm{GeV}/c^2$, selecting only events with produced e^+e^- pairs at rapidity $|y_{\mathrm{ee}}| = 0.5$, the rapidity distribution is flat in a small rapidity region for UPCs and HOs (Appendix 6.1). The hadronic overlaps were simulated with an impact parameter ($\backsim 0 - 4.5$ fm) to account for 0-5 % centrality.
Important to mention is that there are some limitations of these calculations. First of all, higher-order terms are ignored but may be important for calculating the cross-section [22]. Moreover, it is assumed that the nuclei maintain their velocities. Charge stoppings and finite momentum transfers are not included in the calculations, but may also play a role, particularly for HOs [22]. Additionally, STARlight does not take the effects of the impact parameter on the shape of the transverse momentum distribution of the quasi-real photon properly into account. For HOs, this impact parameter dependence can not be neglected [19].

4.3.2 $p_{\mathrm{T,ee}}$- and m_{ee}-spectrum

STARlight outputs the momentum of the single electrons (positrons) from which the momentum and mass of the dielectron ($p_{\mathrm{T,ee}}$ and m_{ee}) can be calculated. In the following, the distributions of both are further examined.

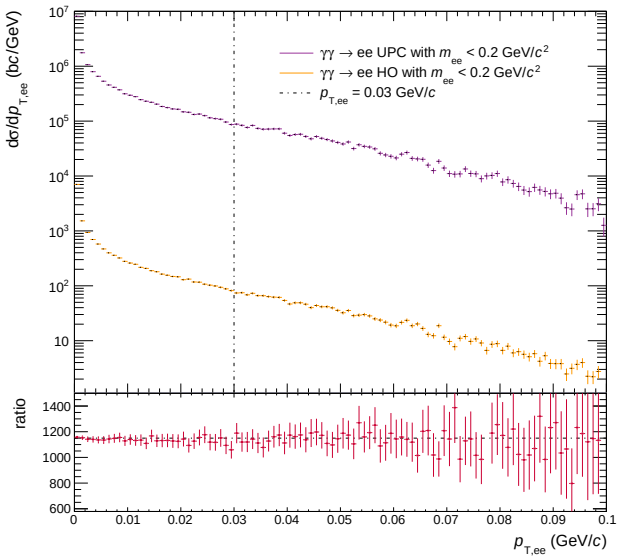

Figure 4.4: $p_{\mathrm{T,ee}}$ distribution for UPCs (violet) and HOs (yellow) with $m_{\mathrm{ee}} < 0.2\mathrm{GeV}/c^2$. The dash-dotted black line denotes $p_{\mathrm{T,ee}} = 0.03\ \mathrm{GeV}/c$. The ratio of the UPC/HO distributions (red) shows that both distributions have a similar shape.

As can be seen in Fig. 4.4, the $p_{\mathrm{T,ee}}$ distributions of both contributions have a similar shape which is expected with STARlight due to the way the impact parameter is handled. They peak at low $p_{\mathrm{T,ee}}$ and are then steeply falling. Only 10.06 % of the UPC distribution is above $p_{\mathrm{T,ee}} = 0.03\ \mathrm{GeV}/c$.
The m_{ee} distribution is shown in Fig. 4.5.

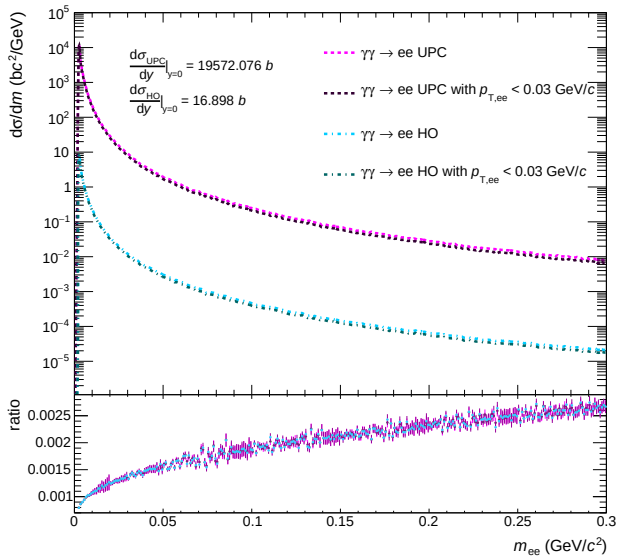

Figure 4.5: m_{ee}-spectrum of UPCs (violet, pink) and HOs (turquoise, blue). The violet and blue lines are the m_{ee}-spectrum with $p_{\mathrm{T,ee}} < 0.03\ \mathrm{GeV}/c$. The ratios of the HO/UPC distributions with and without a $p_{\mathrm{T,ee}}$-cut (violet and blue), shown below, increase slowly.

The electromagnetic backgrounds peak at low m_{ee} and are then steeply falling. The to-

tal cross-sections calculated by STARlight are also shown in the histogram, $\mathrm{d}\sigma/\mathrm{d}y_{\mathrm{UPC}} = 19572.076\,\mathrm{b}$ and $\mathrm{d}\sigma/\mathrm{d}y_{\mathrm{HO}} = 16.898\,\mathrm{b}$. Ultra-peripheral collisions are therefore happening more often than hadronic overlaps or even hadronic collisions ($\sigma_{\mathrm{Pb-Pb(0-5\%)}}$=7.67 b).
Comparing the distribution with and without a selection in $p_{\mathrm{T,ee}}$, one sees that barely anything of the contributions is cut away. Also, 99.9948 % of the UPC distribution are found at $m_{\mathrm{ee}} < 100\,\mathrm{MeV}/c^2$.
Furthermore, the spectra were scaled in such a way that they can be compared with the thermal signal. The different scaling factors are further explained in the following.

4.4 Normalisation

To compare all the background contributions with the thermal signal, they have to be scaled consistently. At the LHC the lead ions are packed into bunches, which are accelerated and then collide with each other, which is called a bunch crossing. The bunch crossings are considered to be happening every 50 ns for Pb-Pb, however, not in every bunch crossing happens a hadronic collision. Furthermore, dielectrons, originating from interactions happening in different bunch crossings, have to be distinguished. Considering the time resolution of the TOF detectors (20 ps), it is possible to select bunch crossings, where a hadronic collision happens, and also distinguish dielectrons from different bunch crossings, therefore, background from different bunch crossings is negligible.
The thermal signal at mid-rapidity ($y_{\mathrm{ee}} = 0$) was calculated for a Pb-Pb collision at $\sqrt{s_{\mathrm{NN}}} = 5.02$ TeV with 0-5 % centrality [16, 17]. The hadronic background produced at $|y_{\mathrm{ee}}| < 0.5$ was accordingly calculated and simulated for a heavy-ion collision with 0-5 % centrality. The electromagnetic backgrounds were also simulated for a Pb-Pb collision selecting only events with produced e^+e^- pairs at rapidity $|y_{\mathrm{ee}}| < 0.5$, but only the HOs were simulated for an impact parameter equivalent to 0-5 % centrality. UPCs on the other hand, happen in Pb-Pb collisions without hadronic collisions and in every bunch crossing, possibly more than one time in a bunch crossing. Thus, part of the UPC background can be rejected by selecting only bunch crossing where at least one hadronic collision happens and by selecting e^+e^- pointing to the primary vertex of the hadronic collision. The corresponding factor by which the UPC mass distribution predicted by STARlight, $\mathrm{d}^2\sigma/\mathrm{d}m_{\mathrm{ee}}\mathrm{d}y$, is suppressed, is called in the following S. This factor (also containing spatial resolution) excludes UPCs not happening in a bunch crossing where one Pb-Pb hadronic collision with 0-5 % centrality occurs

$$S = \mu \cdot 0.05 \cdot \epsilon, \tag{4.8}$$

where μ denotes the possibility that a hadronic collision happens in a bunch crossing (μ=0.01), 0.05 stands for the centrality of the Pb-Pb collision (0-5 % centrality), and ϵ is a factor containing spatial resolution. The UPC background is coming from pile-up interactions from the same bunch crossing in which the hadronic collision happens. The z-distribution, where the two-photon interaction is happening, is assumed to be a Gaussian with $\sigma = 5\,\mathrm{cm}$. Due to the

requirement that the tracks of the electrons point to the primary vertex of the hadronic collision within 5σ, also dielectrons from the UPC pile-up happening within this 5σ surrounding are included. This is given by

$$\epsilon = \frac{\int_{-500\,\mu\mathrm{m}}^{500\,\mu\mathrm{m}} G}{\int_{-10\,\mathrm{cm}}^{10\,\mathrm{cm}} G} = 0.0084, \tag{4.9}$$

where G denotes the z-distribution as gaussian and $5\sigma \mathrel{\widehat{=}} 500\,\mu$m. In the worst case, the hadronic collision and the UPCs happen at the same z vertex. In this case, many dielectrons from pile-up UPCs are included in the 5σ surrounding. This conservative approach was used here to calculate ϵ.
Further, the UPC distribution is scaled with $1/\sigma_{\mathrm{Pb-Pb(0-5\%)}}$ ($\sigma_{\mathrm{Pb-Pb(0-5\%)}}$=7.67 b) to be consistent with the thermal signal, which is given as dielectron yield per hadronic collision with 0-5 % centrality, $\mathrm{d}^2N_{\mathrm{ee}}/\mathrm{d}m_{\mathrm{ee}}\mathrm{d}y$.

4.5 Comparison of contributions

After all of the contributions are normalised consistently, they can be compared to each other. In addition to the hadronic Cocktail, which contains all hadronic background contributions, there is also the background Cocktail (back. Cocktail) containing all backgrounds (hadronic and electromagnetic), and the Cocktail containing all of the measured dielectron yield (backgrounds and thermal signal) which is just called Cocktail in the following. The Cocktails with all background contributions and the thermal signals are shown in Fig. 4.6.

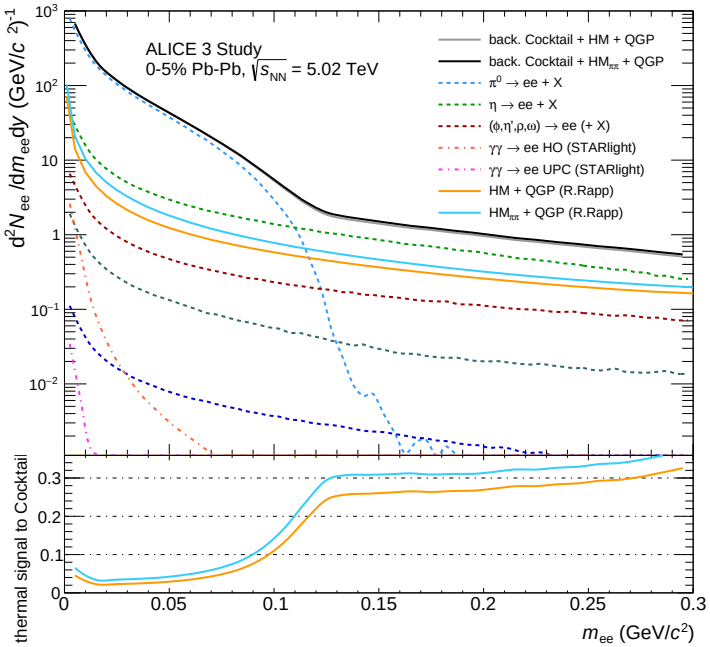

Figure 4.6: All background contributions and the thermal signal are plotted together. The thermal signal is the combined signal of the QGP and HM with and without $\pi\pi$-Bremsstrahlung (blue and orange). The electromagnetic background is the orange (HO) and pink (UPC) dash-dotted line. As expected they peak at low m_{ee}. The black line denotes the sum of all the contributions and the signal of partonic and hadronic matter with $\pi\pi$-Bremsstrahlung. The gray line denotes the same but with hadronic matter without $\pi\pi$-Bremsstrahlung. The ratio shows how much of the Cocktail is actually thermal signal (orange: (HM + QGP)/Cocktail, blue: ($\mathrm{HM}_{\pi\pi}$ + QGP)/Cocktail) [16, 17].

The low m_{ee} region is dominated by the Dalitz decay of the π^0, therefore one would not expect a thermal signal until the pion contribution decreases which happens around $m_{\mathrm{ee}} = 100\,\mathrm{MeV}/c^2$. The electromagnetic backgrounds peak, at low m_{ee} as seen in 4.3.2, but are negligible compared to the pion decay contribution. Since they fall steeply, they are also negligible after the decrease of the π^0 contribution ($m_{\mathrm{ee}} > 100\,\mathrm{MeV}/c^2$) where 20-30 % of the Cocktail is expected to come from the thermal signal.

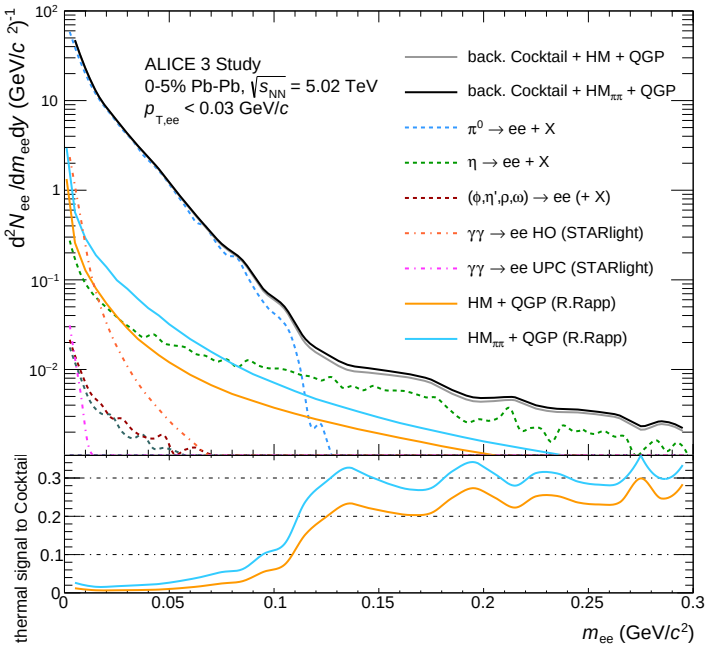

Figure 4.7: The same Cocktails and ratios as above (Fig. 4.6) at low $p_{\mathrm{T,ee}}$ ($p_{\mathrm{T,ee}} < 0.03\,\mathrm{GeV}/c$). The Cocktail falls more steeply and much of the hadronic contributions are cut away. There are also more fluctuations in the hadronic Cocktail [16, 17].

As seen in Fig. 4.7 at low $p_{\mathrm{T,ee}}$ much of the hadronic contributions is cut away. The electromagnetic contributions still peak at low dielectron mass but fall steeply therefore they are also negligible in the intermediate mass region where the thermal signal is expected to be detectable. 20-30 % of the Cocktail still comes from the thermal signal.
In Fig. 4.8 two ratios can be seen. The ratios show the difference between the Cocktail including hadronic matter with $\pi\pi$-Bremsstrahlung and the Cocktail including hadronic matter without $\pi\pi$-Bremsstrahlung, once with a selection in $p_{\mathrm{T,ee}}$ ($p_{\mathrm{T,ee}} < 0.03\,\mathrm{GeV}/c$) and once without.

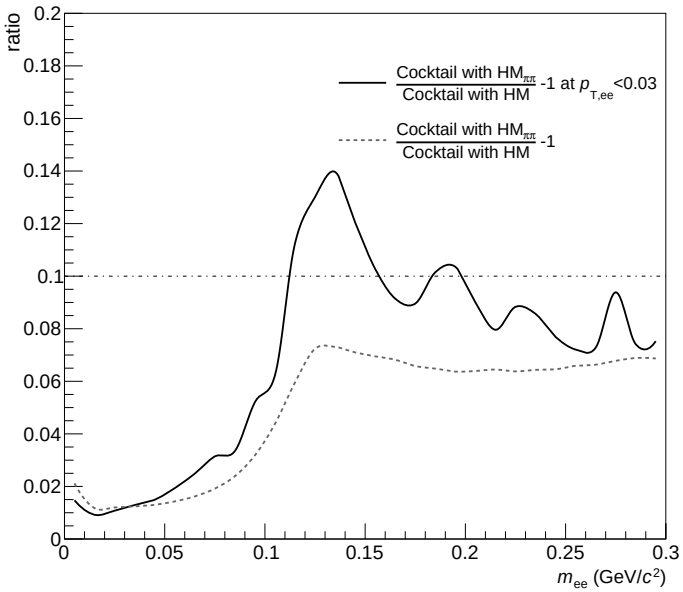

Figure 4.8: Ratios of the Cocktails with the different assumptions for the hadronic matter (Cocktail with HM and Cocktail with $HM_{\pi\pi}$). At low $p_{T,ee}$ (black) and $m_{ee} > 100\,\mathrm{MeV}/c^2$ they differentiate by about $\backsim 10\,\%$ from each other. Without a selection in $p_{T,ee}$ (gray dotted line), they differ by about 6 % [16, 17].

Both Cocktails with different assumptions for the hadronic matter (Cocktail with HM and Cocktail with $HM_{\pi\pi}$) differentiate just by about 6 % from each other without a selection in $p_{T,ee}$. Therefore, it is not likely that they can be distinguished properly. The difference between the predictions for different scenarios (and thus electrical conductivities) in the hadronic phase is larger ($\backsim 10\,\%$) at low $p_{T,ee}$. Hence, one has a better sensitivity to the electrical conductivity at low $p_{T,ee}$.

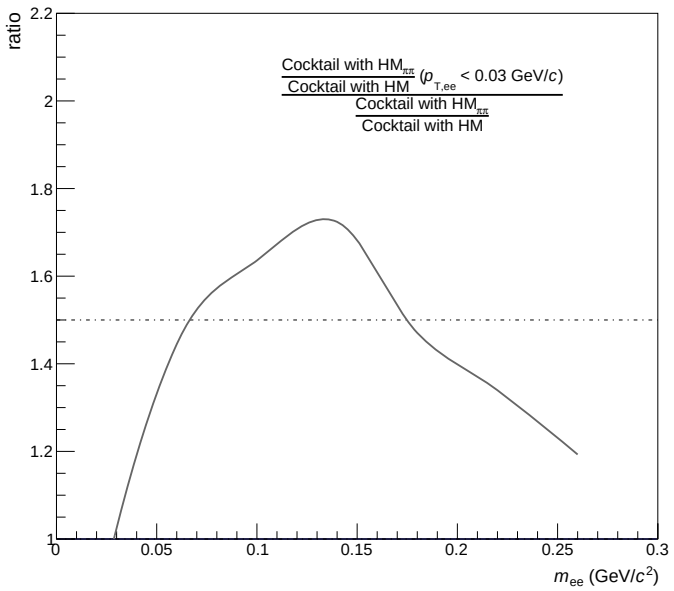

Figure 4.9: The same double ratio as in Fig. 4.2, but now including the background contributions [16, 17].

In Fig. 4.9 the same double ratio as before (Fig. 4.2) was plotted but this time including all the background contributions. Previously, one was more sensitive to the thermal signal at low mass ($0.05\,\mathrm{GeV}/c^2 < m_{\mathrm{ee}} < 0.14\,\mathrm{GeV}/c^2$) but now the peak is relocated to the mass region $0.07\,\mathrm{GeV}/c^2 < m_{\mathrm{ee}} < 0.17\,\mathrm{GeV}/c^2$ because the Dalitz decay of π^0-mesons dominates at low mass ($m_{\mathrm{ee}} < 0.14\,\mathrm{GeV}/c^2$).
Nevertheless, the sensitivity to measure the thermal signal of the partonic and hadronic matter is still better at low $p_{\mathrm{T,ee}}$.

5 Conclusion

In this analysis, a feasibility study for measuring the electrical conductivity of the hot medium created in heavy-ion collisions with ALICE 3 has been conducted. The thermal signal, which can be extracted from the measured dielectron yield, originates from the partonic and hot hadronic matter and is sensitive to the electrical conductivity in this medium. The thermal signal produced at mid-rapidity was calculated for a Pb-Pb collision $\sqrt{s_{\mathrm{NN}}} = 5.02\,\mathrm{TeV}$ with 0-5 % centrality [16, 17]. Since the thermal signal is the combined signal of the partonic and hadronic matter, one needs a good estimation of both. Used in this work were two different assumptions about the signal coming from hadronic matter, once with $\pi\pi$-Bremsstrahlung and once without, which results in two different electrical conductivities. Distinguishing a thermal signal coming from partonic matter and hadronic matter with $\pi\pi$-Bremsstrahlung with one from partonic matter and hadronic matter but without $\pi\pi$-Bremsstrahlung can be enhanced by going to low $p_{\mathrm{T,ee}}$.

There are two different physical background contributions to be considered, namely the hadronic background and the electromagnetic background. The hadronic background contains all dielectrons coming from decaying hadrons, which are produced in the late stage of the heavy-ion collision. This background at mid-rapidity $|y_{\mathrm{ee}}| < 0.5$, was estimated by tuning Monte Carlo simulations to describe measured hadron spectra for a Pb-Pb collision with 0-5 % centrality. The most dominant contribution at low dielectron mass ($m_{\mathrm{ee}} < 0.1\,\mathrm{GeV}/c^2$) are the dielectrons coming from the Dalitz decay of π^0-mesons.

The electromagnetic background arises through the interaction of the Lorenz-contracted electromagnetic fields produced by the colliding nuclei. The interaction can be described via the interaction of photons, which then produce dielectrons ($\gamma\gamma \rightarrow e^+e^-$). There are two possible electromagnetic background interactions: one from pile-up, namely ultra-peripheral collisions (UPC), with an impact parameter bigger than 2 R_{A} (R_{A} = nuclear radius) and one from $\gamma\gamma$ interactions happening on top of the hadronic collisions (HO) with 0-5 % centrality. These backgrounds were simulated with the event generator STARlight for a Pb-Pb collision selecting only events with produced dielectrons at mid-rapidity $|y_{\mathrm{ee}}| < 0.5$ and an impact parameter equivalent to 0-5 % centrality for the HOs. UPCs, in contrast to HOs, happen in Pb-Pb collisions without hadronic collisions and in every bunch crossing. Therefore, the UPC mass distribution is scaled with a suppression factor that includes spatial resolution but also excludes UPCs not happening in a bunch crossing where one Pb-Pb hadronic collision with 0-5 % centrality occurs.

After comparing all background contributions to the thermal signal, one sees that the electromagnetic backgrounds peak at low $p_{\mathrm{T,ee}}$ and m_{ee}, but are negligible above $m_{\mathrm{ee}} > 100\,\mathrm{MeV}/c^2$. The hadronic backgrounds dominate the spectrum at $m_{\mathrm{ee}} < m_{\pi^0}$. Hence, one expects to be most sensitive to the thermal signal at $m_{\mathrm{ee}} > m_{\pi^0}$, where the thermal signal is about 20-30 % of the total dielectron yield. Nonetheless, the sensitivity to σ_{el} is larger at low $p_{\mathrm{T,ee}}$.

The next steps of this analysis would be, to conduct acceptance and efficiency studies with the acceptances and efficiencies of the detectors that are considered to be used for ALICE 3. Furthermore, more sophisticated studies including the combinatorial background are needed, to better evaluate the feasibility of measuring a signal of the electrical conductivity of the partonic and hadronic matter.

6 Appendix

6.1 Rapidity distribution of ultra-peripheral collisions and hadronic overlaps

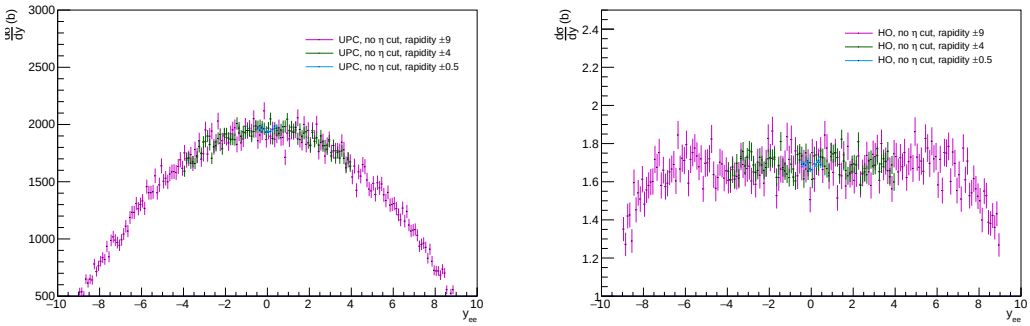

Figure 6.1: The rapidity distribution for UPCs (left) and HOs (right) simulated in different rapidity regions ($y_{\mathrm{ee}} = \pm 8$ (pink), $y_{\mathrm{ee}} = \pm 4$ (green) and $y_{\mathrm{ee}} = \pm 0.5$ (blue)) with no selection in η. For a small rapidity ($y_{\mathrm{ee}} = \pm 0.5$) region both distributions are relatively flat.

References

[1] *Standard model of particle physics.* URL: https://upload.wikimedia.org/wikipedia/commons/thumb/0/00/Standard_Model_of_Elementary_Particles.svg/627px-Standard_Model_of_Elementary_Particles.svg.png. (last accessed on: 17.04.2023).

[2] CMS Collaboration. "Measurement of the inclusive 3-jet production differential cross section in proton–proton collisions at 7 TeV and determination of the strong coupling constant in the TeV range". In: *The European Physical Journal C* 75.5 (May 2015). DOI: 10.1140/epjc/s10052-015-3376-y. URL: https://doi.org/10.1140%2Fepjc%2Fs10052-015-3376-y.

[3] Rupa Chatterjee, Lusaka Bhattacharya, and Dinesh K. Srivastava. "Electromagnetic Probes". In: *The Physics of the Quark-Gluon Plasma.* Springer Berlin Heidelberg, 2009, pp. 219–264. DOI: 10.1007/978-3-642-02286-9_7. URL: https://doi.org/10.1007%2F978-3-642-02286-9_7.

[4] Norman M. Kroll and Walter Wada. "Internal Pair Production Associated with the Emission of High-Energy Gamma Rays". In: *Phys. Rev.* 98 (5 June 1955), pp. 1355–1359. DOI: 10.1103/PhysRev.98.1355. URL: https://link.aps.org/doi/10.1103/PhysRev.98.1355.

[5] PHENIX Collaboration. "Detailed measurement of the e+e- pair continuum in p+p and Au+Au collisions at $\sqrt{s_{NN}} = 200$ GeV and implications for direct photon production". In: 81.3 (Mar. 2010). DOI: 10.1103/physrevc.81.034911. URL: https://doi.org/10.1103%5C%2Fphysrevc.81.034911.

[6] L. D. McLerran and T. Toimela. "Photon and dilepton emission from the quark-gluon plasma: Some general considerations". In: *Phys. Rev. D* 31 (3 Feb. 1985), pp. 545–563. DOI: 10.1103/PhysRevD.31.545. URL: https://link.aps.org/doi/10.1103/PhysRevD.31.545.

[7] Hendrik van Hees and Ralf Rapp. "Comprehensive Interpretation of Thermal Dileptons Measured at the CERN Super Proton Synchrotron". In: *Physical Review Letters* 97.10 (Sept. 2006). DOI: 10.1103/physrevlett.97.102301. URL: https://doi.org/10.1103%2Fphysrevlett.97.102301.

[8] Hendrik van Hees. "Renormierung selbstkonsistenter Näherungen in der Quantenfeldtheorie bei endlichen Temperaturen". PhD thesis. Darmstadt: Technische Universität, Dec. 2000. URL: http://tuprints.ulb.tu-darmstadt.de/82/.

[9] *Heaviside-Funktion.* URL: https://de.wikipedia.org/wiki/Heaviside-Funktion. (last accessed on: 16.07.2023).

[10] Nan Su. "A Brief Overview of Hard-Thermal-Loop Perturbation Theory". In: *Communications in Theoretical Physics* 57.3 (Mar. 2012), pp. 409–421. DOI: 10.1088/0253-6102/57/3/12. URL: https://doi.org/10.1088%2F0253-6102%2F57%2F3%2F12.

[11] Charles Gale and Joseph I. Kapusta. "Vector dominance model at finite temperature". In: *Nuclear Physics B* 357.1 (1991), pp. 65–89. ISSN: 0550-3213. DOI: https://doi.org/10.1016/0550-3213(91)90459-B. URL: https://www.sciencedirect.com/science/article/pii/055032139190459B.

[12] Guy D. Moore and Jean-Marie Robert. "Dileptons, spectral weights, and conductivity in the Quark-Gluon Plasma". In: (2006). arXiv: hep-ph/0607172 [hep-ph].

[13] Moritz Greif et al. "Electric conductivity of the quark-gluon plasma investigated using a perturbative QCD based parton cascade". In: *Physical Review D* 90.9 (Nov. 2014). DOI: 10.1103/physrevd.90.094014. URL: https://doi.org/10.1103%5C%2Fphysrevd.90.094014.

[14] Jan Hammelmann et al. "Electrical conductivity and relaxation via colored noise in a hadronic gas". In: (Oct. 2018).

[15] ALICE Collaboration. "Letter of intent for ALICE 3: A next-generation heavy-ion experiment at the LHC". In: (Nov. 2022). arXiv: 2211.02491 [physics.ins-det].

[16] Ralf Rapp. "Dilepton Spectroscopy of QCD Matter at Collider Energies". In: *Adv. High Energy Phys.* 2013 (2013), p. 148253. DOI: 10.1155/2013/148253. arXiv: 1304.2309 [hep-ph].

[17] Ralf Rapp. "EMMI Rapid Reaction Task Force (RRTF): Electric conductivity and soft EM radiation in hadronic matter". In: (13.06.2021). URL: https://indico.gsi.de/event/12989/.

[18] ALICE Collaboration. "Production of charged pions, kaons, and (anti-)protons in Pb-Pb and inelastic *pp* collisions at $\sqrt{s_{NN}} = 5.02$ TeV". In: *Phys. Rev. C* 101 (4 Apr. 2020), p. 044907. DOI: 10.1103/PhysRevC.101.044907. URL: https://link.aps.org/doi/10.1103/PhysRevC.101.044907.

[19] ALICE Collaboration. "Dielectron production at midrapidity at low transverse momentum in peripheral and semi-peripheral Pb−Pb collisions at $\sqrt{s_{\mathrm{NN}}} = 5.02$ TeV". In: *Journal of High Energy Physics* (2022). arXiv: 2204.11732 [nucl-ex].

[20] *STARlight*. URL: https://en.wikipedia.org/wiki/STARlight#cite_note-3. (last accessed on: 16.07.2023).

[21] Spencer R. Klein et al. "STARlight: A Monte Carlo simulation program for ultra-peripheral collisions of relativistic ions". In: *Computer Physics Communications* 212 (Mar. 2017), pp. 258–268. DOI: 10.1016/j.cpc.2016.10.016. URL: https://doi.org/10.1016%5C%2Fj.cpc.2016.10.016.

[22] J. D. Brandenburg, W. Zha, and Z. Xu. "Mapping the electromagnetic fields of heavy-ion collisions with the Breit-Wheeler process". In: *The European Physical Journal A* 57.10 (Oct. 2021). DOI: 10.1140/epja/s10050-021-00595-5. URL: https://doi.org/10.1140%2Fepja%2Fs10050-021-00595-5.

Danksagung

Zuerst möchte ich Prof. Harald Appelshäuser für seine Unterstützung danken und die Möglichkeit, in der Frankfurter ALICE Arbeitsgruppe meine Bachelorarbeit zu schreiben.

Bei Sebastian Scheid möchte ich mich für die Betreuung und für die viele Unterstützung bedanken.

Des Weiteren danke ich Dr. Raphaelle Bailhache für ihre Betreuung und Jerome Jung für zahlreiche Hilfestellungen.

Emma Ege möchte ich für die vielen konstruktiven Gespräche danken.

Als letztes bedanke ich mich bei der gesamten Arbeitsgruppe für das angenehme und lustige Arbeitsumfeld, sowie bei meinen Eltern, die mich immer unterstützt haben.

Selbstständigkeitserklärung

Erklärung nach §30 (12) Ordnung für den Bachelor- und den Masterstudiengang

Hiermit erkläre ich, dass ich die Arbeit selbstständig und ohne Benutzung anderer als der angegebenen Quellen und Hilfsmittel verfasst habe. Alle Stellen der Arbeit, die wörtlich oder sinngemäß aus Veröffentlichungen oder aus anderen fremden Texten entnommen wurden, sind von mir als solche kenntlich gemacht worden. Ferner erkläre ich, dass die Arbeit nicht - auch nicht auszugsweise - für eine andere Prüfung verwendet wurde.

Frankfurt, den

Clara Melisande Peter